

Quantum Modeling, Part I : Poisson-Schrodinger Solver

1. Introduction

The trend toward smaller MOSFET devices with thinner gate oxide and greater doping is resulting in the increased importance of quantum mechanical effects, which are observed as shifts in threshold voltage and gate capacitance. Predicting these quantum effects requires solving the Schrodinger equation. This article (part 1 of a series) presents the Poisson-Schrodinger solver and its enhancements implemented in *ATLAS* from Silvaco. Section 2 presents the syntax used to perform the simulation. Section 3 presents the MOS-capacitor simulation results and compares them with results obtained with the University of Pisa code [1-6].

2. Poisson-Schrodinger Solver in ATLAS

To consistently solve Poisson and Schrodinger equations with *ATLAS*, the user must specify different parameters in the MODELS statement:

```
models fermi schro new.eig ox.poisson \
  qy.min=<val> qy.max=<val> \
  qx.min=<val> qx.max=<val> \
  ox.schro fixed.fermi
```

fermi specifies the Fermi-Dirac statistics, *schro* sets the Schrodinger solver for electrons, *ox.poisson* specifies the oxide to be considered as a semiconductor,

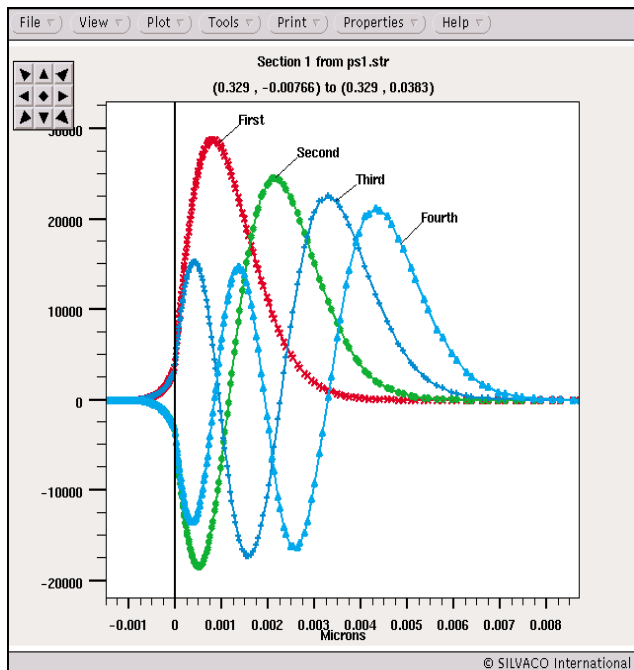


Figure 2. The first 4 eigenfunctions for the electron longitudinal mass near the interface oxide/silicon (in $m^{-1/2}$).

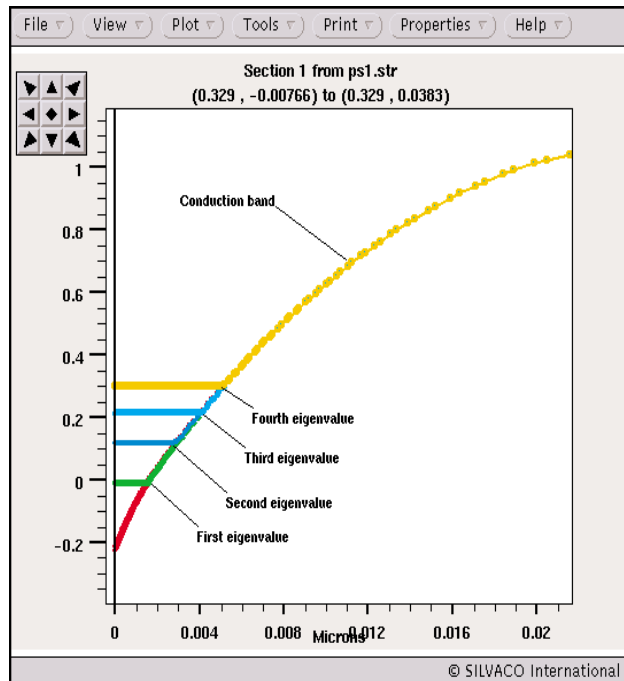


Figure 1. The first 4 eigenvalues for the electron longitudinal effective mass and the conduction band (in eV).

new.eig specifies the new eigensolver, *ox.schro* indicates that the silicon oxide is included in the Schrodinger domain, (*qx.min*, *qx.max*, *qy.min*, *qy.max*) define a box where the Schrodinger equation is solved, *fixed.fermi* sets the quasi-fermi levels to zero, *disp* sets the type of eigenvalues/vectors to display. The new parameters *new.eig*, *ox.poisson* *qx.min*, *qx.max*, *qy.min*, *qy.max*, *ox.schro* are explained below.

A new eigensolver is implemented in *ATLAS* that exhibits a better convergence and speed than the previous version. The eigenvalues finder is based on the QL-algorithm for tridiagonal matrices and the eigenvector finder based on the inverse iteration method. Since the potential at the edges of the Schrodinger domain is considered infinite and only silicon is considered, the oxide should be included in the Schrodinger domain with *ox.schro* in order to take into account the actual barrier at the oxide/silicon interface. This approach lets eigenfunctions penetrate into the oxide. The quantum box should be defined (with *qx.min*, *qx.max*, *qy.min*, *qy.max*) so that *qy.min* is within the oxide. Finally, the flag *ox.poisson* indicates that the charge in the oxide, like a semiconductor, is included in the Poisson equation.

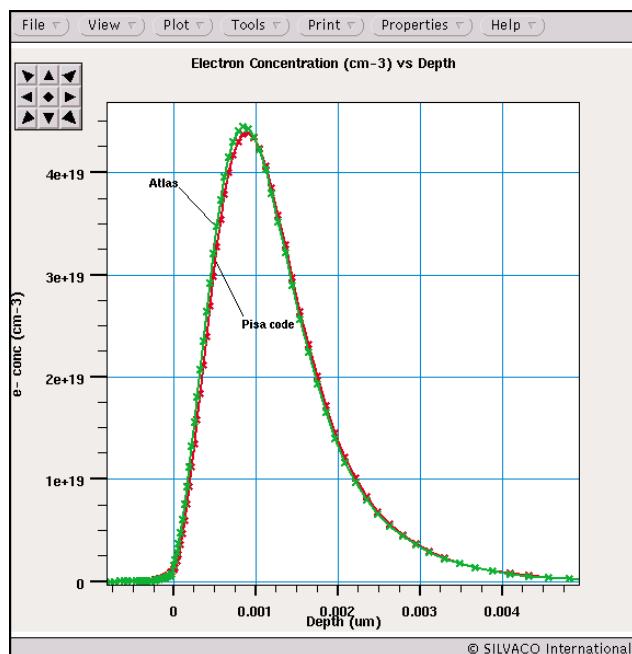


Figure 3. Electron concentration vs depth. The red curve is from the Pisa code and the green one from ATLAS.

The user may now set new material parameters for the effective masses and degeneracy factor. The default values in silicon and silicon oxide are:

```
material material=silicon ml=0.98 \
  mt1=0.19 mt2=0.19 mhh=0.49 \
  mlh=0.16 degeneracy=2
material material=sio2 ml=0.3 mt1=0.3 \
  mt2=0.3 mhh=1 mlh=1 degeneracy=1
```

ml is the electron effective longitudinal mass, mt1 and mt2 are the electron transverse effective masses, mlh and mhh are the effective masses of light and heavy holes, and degeneracy is the degeneracy factor. The Schrodinger solver for holes and their effective masses is used when p.schro is set in the MODELS statement.

Finally, before applying a bias on the electrodes, the user should specify the Poisson and Schrodinger equations to solve and disable the continuity equations:

```
method carriers=0
```

3- Results

A p-type MOS-capacitor was defined in ATLAS. Silicon is $2.5e18 \text{ cm}^{-3}$ p-type doped, and the gate oxide is 1.5 nm thick. For 1V applied on the gate while in inversion mode, Figures 1 and 2 show the first 4 eigenvectors and eigenvalues related to the longitudinal effective mass. The $x=0$ coordinate on these figures stand for the oxide/silicon interface. Figure 2 shows the clear penetration of the eigenfunctions in the oxide.

Figure 3 displays the relatively good agreement between electron concentration (for $V_{gate}=1V$) and its comparison to the electron concentration obtained with the code of the University of Pisa. Then, in Figure 4, this electron concentration is compared with the one obtained after a semi-classical simulation. This overlay shows that the maximum of the electron concentration is beneath the interface in the quantum case and its value is smaller than the semi-classical case. This position is directly linked to the position of the maximum of the electron probability distribution given by the first eigenvector (red curve in Figure 2).

As commonly used, one can also perform C(V) curves. In ATLAS, the low frequency C(V) curve can be computed in static operation: the charge concentration is integrated in the whole structure and then this quantity is derived as $C=-dQ/dV$. To get the charge in the output file the user should specify the charge parameter in the OUTPUT statement. The integrated net charge will be saved in a logfile with the help of the probe command:

```
probe name=charge charge integrate left=0.0 right=1.0 \
  top=0.0 bottom=1.0
```

where (left, right, top, bottom) are the edges of the silicon region.

Then, the capacitance is computed using the EXTRACT command in DeckBuild:

```
extract name="dQdV" \
  deriv(v."gate", -1e-04*probe."charge") \
  outfile="CV.out"
```

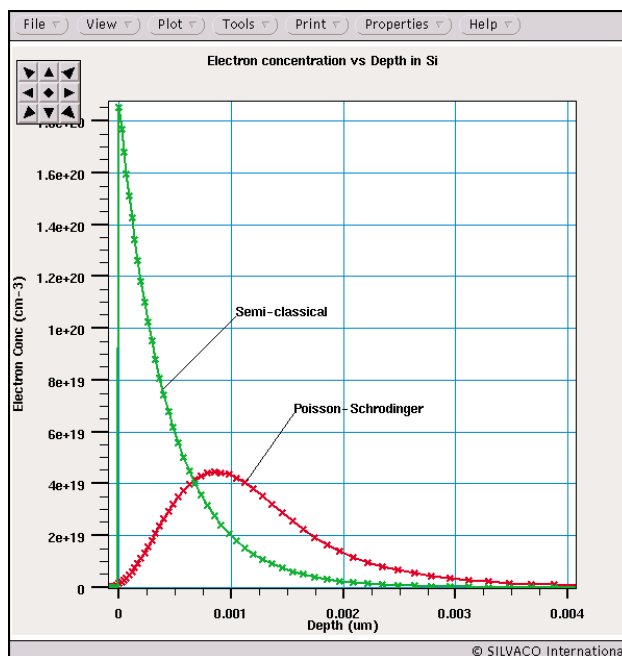


Figure 4. Electron concentration vs depth for semi-classical (green curve) and Poisson-Schrodinger (red curve) models.

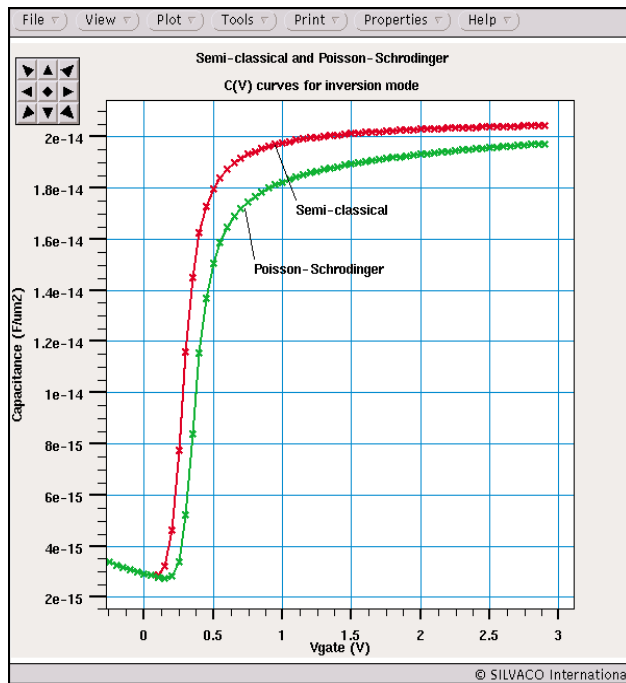


Figure 5: comparison of the semi-classical and Poisson-Schrodinger C(V) curves in inversion mode.

The $1e-04$ factor gives the capacitance in $F/\mu m^2$.

Figure 5 illustrates the overlay of the semi-classical and quantum C(V) curves for the same p-type MOS-capacitor as previously described. In inversion mode, the quantum capacitance is smaller than the semi-classical capacitance; this effect is expressed like a thicker effective oxide in a quantum case, rather than the actual oxide obtained in semi-classical case. The electron depletion region beneath the interface showed in Figure 4 explains it. Figure 6 shows the good agreement obtained with an *ATLAS* comparison of the quantum C(V) curve and the University of Pisa code.

4- Conclusion

This paper has presented the new features of *ATLAS* dealing with Poisson-Schrodinger simulations, including a new eigensolver that takes into account the silicon oxide, the different effective masses, and the degeneracy factors for silicon and silicon oxide. This solver has shown good results when compared to the code of the University of Pisa. This solver extends to nonplanar structures originating in the Silvaco process simulator *ATHENA* by adding the `new.schro` parameter in the `MODELS` statement. We have shown in this paper that *ATLAS* now includes an accurate Poisson-Schrodinger solver. In Part II of the article this model will be used to calibrate the Density Gradient model. Part II will be presented in a future *Simulation Standard* issue.

References

- [1] G.Iannaccone, M.Macucci, P.Coli, G.Curatola, G.Fiori, M.Gattobigio, M.Pala, "Towards nanotechnology computer aided design: the NANOCAD project", IEEE-NANO 2001.
- [2] G.Fiori, G.Iannaccone, "The effect of quantum confinement and discrete dopants in nanoscale 50nm n-MOSFETs: a three-dimensional simulation", Nanotechnology 13 (2002) 294-298.
- [3] G.Fiori, G.Iannaccone et al., "Experimental and Theoretical investigation of quantum point contacts for the validation of models for surface states", Nanotechnology 13 (2002) 299-303.
- [4] G.Fiori, G.Iannaccone, "Effects of quantum Confinement and discrete dopants in nanoscale bulk-Si nMOSFET", IEEE-NANO 2001.
- [5] G.Fiori, G.Iannaccone, "Modeling of ballistic nanoscale metal-oxide-semiconductor field effect transistors", Applied Physics Letters, vol.81, 19, Nov.2002.
- [6] G.Iannaccone, G.Fiori, G.Curatola, "Techniques and methods for the simulation of nanoscale ballistic MOSFETs", IEEE-NANO 2002.

We thank the University of Pisa for its data and contribution to this work.

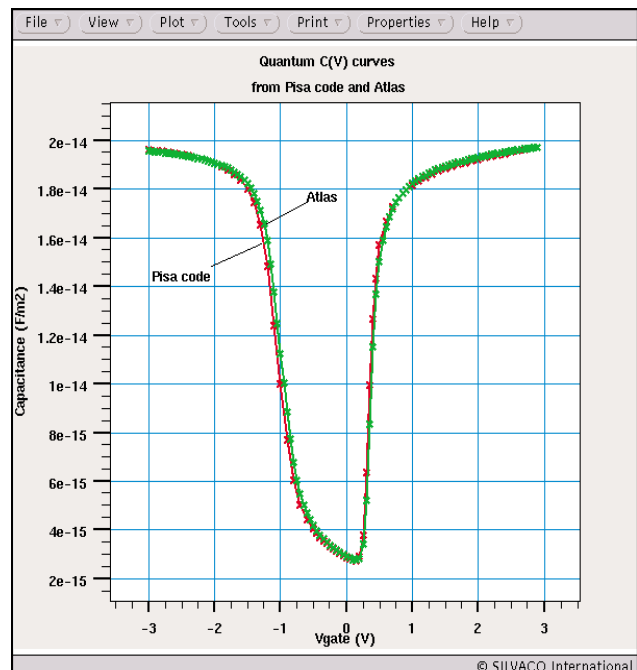


Figure 6. Comparison of the C(V) curves obtained from Pisa code (red curve) and *ATLAS* (green curve).